The EU Framework Programme for Research and Innovation H2020
Research and Innovation Action

CENTAURO

Deliverable D2.4 Balance and wheeled locomotion control strategies

Dissemination Level: Public

Project acronym:	CENTAURO
Project full title:	Robust Mobility and Dexterous Manipulation in Disaster Response by Fullbody Telepresence in a Centaur-like Robot
Grant agreement no.:	644839
Lead beneficiary:	IIT – Fondazione Istituto Italiano di Tecnologia
Authors:	Malgorzata Kamedula, Navvab Kashiri and Nikos Tsagarakis
Work package:	WP2 – Robot Platform
Date of preparation:	2017-08-01
Type:	Report
Version number:	1.0

Document History

Version	Date	Author	Description
0.1	2017-07-30	Małgorzata Kamedula, Navvab Kashiri and Nikos Tsagarakis	Initial version
0.2	2017-08-01	Navvab Kashiri	revised version
1.0	2017-09-02	Navvab Kashiri, and Nikos Tsagarakis	Submission version

Executive Summary

Within WP2 the main control activities during the second half of the project was related to the whole-body control of the CENTAURO robot. The first main result from this effort is the wheeled control of the CENTAURO robot. This report provides the details of the whol-body controller and wheeled motion control scheme accounting for series elastic torque-controlled actuators developed within WP2. In particular, the report presents an overview of the balancing control, as well as kinematics control for steering strategies. Finally, simulation results presenting the functionality of proposed scheme in performing balancing, and executing various locomotion trajectories through wheel motions are displayed.

Contents

1 Introduction

This report describes the development of tasks 2.3 and 2.4 from WP2 related to whole-body control, balancing, and wheeled motion. The methods adopted for these tasks are described, and important implementation details are pointed out. Then, the CENTAURO simulation results are presented to validate selected approaches[1].

In the first section, implemented controller scheme is described starting from a centralised controller, through an inverse kinematics resolution to operational-space and balancing tasks; while the second section proposes a wheeled motion scheme.

2 Whole-body Control and Balancing

In this section we present a scheme for the whole-body control of the CENTAURO robot and eventually utilise it for balancing. The CENTAURO robot design offers multiple operation modes including legged, wheeled, and combined locomotion. Moreover, depending on the task, various conditions may arise that impose/release a set of constraints on body states. To fully exploit the robot potential, the control scheme needs to be capable of adapting to such changes while respecting joint state limits on kinematic and dynamic levels. To this end, an operational space control [20] is often employed to deal with redundant systems, e.g. in case of quadrupeds [16], [36], or manipulators [9], [32].

The literature presents several measures to evaluate the system stability that includes the most widely recognised centre of mass (CoM) position, zero moment point (ZMP) and centre of pressure (CoP) [31]. Most research on the stability of legged robots have been dedicated to bipeds, e.g. [15, 17, 18, 23], while quadrupeds, as statically stable systems, have attracted less attention. Nevertheless, an extension of methods developed for humanoid robots to multi-legged systems is not always straightforward because additional factors such as workspace limitations and discontinuities in a support polygon have to be taken into account [21, 22]. Moreover, commonly used models in humanoids [24, 39, 40] and their extensions to quadrupeds [3, 11, 26] are not directly applicable to the CENTAURO robot due to its non-negligible leg dynamics, and the upper-body structure. In this work, we employ the CoM regulation for the CENTAURO robot balancing, that relies upon the whole-body control scheme to be detailed in next sections.

2.1 Floating-base Model of Leg-Wheeled Robots

In derivation of control schemes, a floating base model can be used with generalised coordinates[2]

$$\bar{\boldsymbol{q}} = \begin{bmatrix} \bar{\boldsymbol{q}}_b^T & \boldsymbol{q}_a^T \end{bmatrix}^T, \tag{1}$$

where $\bar{\boldsymbol{q}}_b \in \{\mathrm{SE}^3 \mid \Re^{n_b}\}$ refers to coordinates of any floating base representation, $n_b \in \mathbb{N}$ denotes the size of the floating base coordinates vector, and $\boldsymbol{q}_a \in \Re^{n_a}$ represents the vector of link-side positions of actuated joints with $n_a \in \mathbb{N}$ symbolising the number of actuated joints.

[1] The videos associated with the simulations carried out in this work are available at `https://www.youtube.com/playlist?list=PLGYQZBk-v9IpojZXxGSoptThRbd65P12N`

[2] In this document, ${}^0(.)_1^{(2)}$ denotes a state vector from a point 0 to a point 1 expressed in a reference frame 2. Its simplified version ${}^0(.)_1$ represents a state vector from a point 0 to a point 1 expressed in any reference frame, and it is used whenever a formula does not depend on a specific reference frame. A symbol $(.)_1^{(0)}$ indicates the state $(.)$ of a point 1 expressed in a reference frame 0, and $(.)_{des}$ stands for the desired value of $(.)$. Finally, multiple subscripts/superscripts are comma separated.

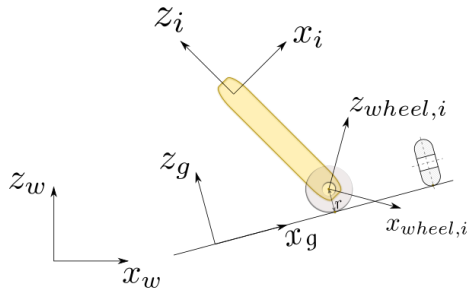

Figure 1: Reference frames arrangement for the contact point position estimation in the legged-wheeled structure.

Therefore, the overall system is described by $n_c = n_a + n_b$ coordinates. We can also define a new set of generalised coordinates

$$\boldsymbol{q} = \begin{bmatrix} \boldsymbol{q}_b^T & \boldsymbol{q}_a^T \end{bmatrix}^T, \tag{2}$$

with $\boldsymbol{q}_b \in \{\mathrm{SE}^3 \mid \Re^6\}$ denoting the floating base coordinates, and $\boldsymbol{q} \in \Re^n$ with $n = n_a + 6$ therefore holds. The system's dynamic model can then be presented by

$$\mathbf{M}(\bar{\boldsymbol{q}})\ddot{\boldsymbol{q}} + \boldsymbol{c}(\bar{\boldsymbol{q}}, \dot{\boldsymbol{q}}) + \boldsymbol{g}(\bar{\boldsymbol{q}}) = \mathbf{S}^T \boldsymbol{\tau}_t(\boldsymbol{q}_a, \dot{\boldsymbol{q}}_a, \boldsymbol{\theta}, \dot{\boldsymbol{\theta}}) + \mathbf{J}_c^T(\bar{\boldsymbol{q}})\boldsymbol{\lambda}, \tag{3}$$

where $\mathbf{M} \in \Re^{n \times n}$ stands for the corresponding generalised inertia matrix, $\boldsymbol{c} \in \Re^n$ represents Coriolis/centrifugal forces, $\boldsymbol{g} \in \Re^n$ denotes the gravitational torque vector, $\boldsymbol{\tau}_t \in \Re^{n_a}$ is the vector of transmission torques, and $\boldsymbol{\theta} = [\theta_1, ..., \theta_{n_a}]^T$ refers to the motor position vector. $\mathbf{S} = \begin{bmatrix} \mathbf{0}^{n_a \times n_b} & \mathbf{I}^{n_a \times n_a} \end{bmatrix}$ symbolises the actuation selection matrix, $\mathbf{J}_c \in \Re^{k \times n}$ describes the constraints Jacobian, and $\boldsymbol{\lambda} \in \Re^k$ stands for reaction forces with $k \in \mathbb{N}$ expressing the number of system constraints.

2.2 Ground Centralised Controller

Each feet in contact with the ground is modelled using point-contact assumption as follows

$$^w\dot{\boldsymbol{x}}_{c,i} = \mathbf{0}, \tag{4}$$

with $^w\boldsymbol{x}_{c,i} \in \Re^3$ expressing the position vector from the world frame origin to the i_{th} leg contact point.

For a hybrid legged-wheeled system, in contrary to legged-robots with point feet (with negligible foot geometry) or standard wheeled platforms (with fixed placement of wheels w.r.t limbs), it is not possible to define a constant transformation between a wheel-ground contact point and a body reference frame , see Fig. 1. Nevertheless, by assuming zero camber angle and known ground orientation, the contact point position for the i_{th} leg can be computed based on the system kinematics

$$\boldsymbol{x}_{c,i}^{(g)} = \boldsymbol{x}_{wheel,i}^{(g)} - \begin{bmatrix} 0 & 0 & r \end{bmatrix}^T, \tag{5}$$

where $\boldsymbol{x}_{wheel,i}$ represents the i^{th} wheel centre, $\boldsymbol{x}_{c,i}$ symbolises the i^{th} leg contact point and r stands for the wheel radius. The contact constraints (4) can then be rewritten in a form

$$^w\dot{\boldsymbol{x}}_{c,i} = \mathbf{J}_{c,i}\dot{\boldsymbol{q}} = \vec{0}, \tag{6}$$

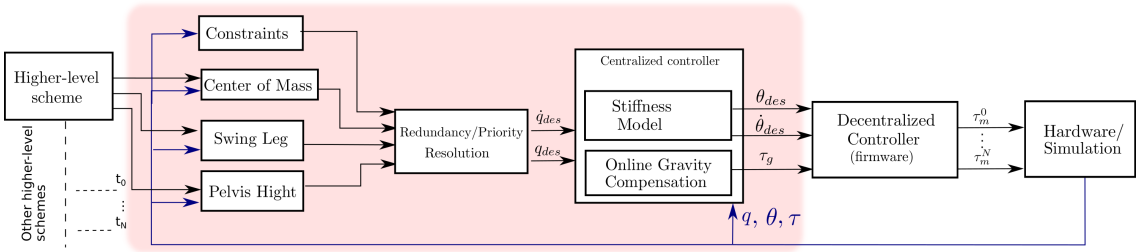

Figure 2: Scheme of the controller structure in the legged motion set-up.

with $\mathbf{J}_{c,i} \in \Re^{3\times n}$ denoting the i^{th} leg constraints Jacobian. Finally, the overall constraints Jacobian ($\mathbf{J}_c \in \Re^{3f\times n}$) for wheels with ground contactis described by

$$\mathbf{J}_c = \begin{bmatrix} \mathbf{J}_{c,1} \\ \vdots \\ \mathbf{J}_{c,f} \end{bmatrix}. \tag{7}$$

The contact constraint Jacobian $\mathbf{J}_c$ can also be expressed in a following form

$$\mathbf{J}_c = \begin{bmatrix} \mathbf{J}_{c1} & \mathbf{J}_{c2} & \mathbf{J}_{c3} \end{bmatrix}, \tag{8}$$

where $f \in \mathbb{N}$ denotes the number of legs with ground contact, $\mathbf{J}_{c3} \in \Re^{6\times f}$ symbolises the part of the Jacobian related to driving DoFs, $\mathbf{J}_{c2} \in \Re^{6\times f}$ stands for the part related to ankles yaw DoFs, and $\mathbf{J}_{c1} \in \Re^{6\times(n-2f)}$ represents the remaining part of the constraints Jacobian.

2.3 Gravity Compensation for Compliant Joint Legged Robots

The scheme developed for the CENTAURO robot control is depicted in Fig. 2. The input of the decentralised impedance/torque controller, presented in [19], is obtained from a centralised controller to ensure accurate tracking of given references while replicating low or high impedance behaviours. The centralised controller utilised in this work executes flexible-joint gravity compensation, and therefore relies upon two components: rigid-joint gravity compensation and elasticity model. Derivation of the former for robots subject to contact constraints, e.g. legged robots or manipulators

in contact with environment, the external forces in the dynamic equation (3) have to be considered. Over the years, several solutions based on an orthogonal decomposition of the constraints Jacobian have been proposed to address this issue including [25], [1], and [2]. In this work, a QR decomposition of the constraints Jacobian is used, as shown in [27]. It can be expressed by

$$\mathbf{J}_c^T(\boldsymbol{q}) = \mathbf{Q}(\boldsymbol{q})\mathbf{R}(\boldsymbol{q}) \tag{9}$$

where $\mathbf{Q} \in \Re^{n\times n}$ is an orthogonal matrix, and $\mathbf{R} \in \Re^{n\times k}$ is an upper triangular matrix with $\text{rank}(\mathbf{R}) = l$; l denotes number of independent constraints. Then, by applying (9) on (3), one can obtain an equivalent dynamic model as

$$\mathbf{S}_c\mathbf{Q}^T(\boldsymbol{q})\left(\mathbf{M}(\boldsymbol{q})\ddot{\boldsymbol{q}} + \boldsymbol{c}(\boldsymbol{q},\dot{\boldsymbol{q}}) + \boldsymbol{g}(\boldsymbol{q})\right) = \mathbf{S}_c\mathbf{Q}^T(\boldsymbol{q})\mathbf{S}^T\boldsymbol{\tau} + \mathbf{R}\boldsymbol{\lambda}, \tag{10}$$

$$\mathbf{S}_u\mathbf{Q}^T(\boldsymbol{q})\left(\mathbf{M}(\boldsymbol{q})\ddot{\boldsymbol{q}} + \boldsymbol{c}(\boldsymbol{q},\dot{\boldsymbol{q}}) + \boldsymbol{g}(\boldsymbol{q})\right) = \mathbf{S}_u\mathbf{Q}^T(\boldsymbol{q})\mathbf{S}^T\boldsymbol{\tau}, \tag{11}$$

where $\mathbf{S}_c = \begin{bmatrix} \mathbf{I}^{l\times l} & \mathbf{0}^{l\times(n-l)} \end{bmatrix}$ expresses a selection matrix for the constrained part of the system dynamics, and $\mathbf{S}_u = \begin{bmatrix} \mathbf{0}^{(n-l)\times l} & \mathbf{I}^{(n-l)\times(n-l)} \end{bmatrix}$ stands for a selection matrix of the unconstrained part of the system dynamics.

The rigid-joint gravity compensation torque ($\boldsymbol{\tau_g} \in \Re^{n_a}$) can then be defined as

$$\boldsymbol{\tau_g}(\boldsymbol{q}) = (\mathbf{S}_u\mathbf{Q}^T(\boldsymbol{q})\mathbf{S}^T)^+\mathbf{S}_u\mathbf{Q}^T(\boldsymbol{q})\boldsymbol{g}(\boldsymbol{q}), \tag{12}$$

which is constructed based only on the contact points positions, in addition to typical model parameters, and the external force measurement/estimation is not needed.

To account for joint compliance, it is essential to recall the corresponding dynamics, which can be expressed by

$$\mathbf{B}_m\ddot{\boldsymbol{\theta}} + \mathbf{D}_m\dot{\boldsymbol{\theta}} + \boldsymbol{\tau}_t(\boldsymbol{q}_a, \dot{\boldsymbol{q}}_a, \boldsymbol{\theta}, \dot{\boldsymbol{\theta}}) = \boldsymbol{\tau}_m, \tag{13}$$

$$\boldsymbol{\tau}_t(\boldsymbol{q}_a, \dot{\boldsymbol{q}}_a, \boldsymbol{\theta}, \dot{\boldsymbol{\theta}}) = \mathbf{K}_t(\boldsymbol{\theta} - \boldsymbol{q}_a) + \mathbf{D}_t(\dot{\boldsymbol{\theta}} - \dot{\boldsymbol{q}}_a), \tag{14}$$

where $\mathbf{K}_t \in \Re^{n_a \times n_a}$ and $\mathbf{D}_t \in \Re^{n_a \times n_a}$ stand for the stiffness and damping matrices corresponding to the passive elements, whereas $\boldsymbol{\tau}_m \in \Re^{n_a}$ denotes the motor torque vector, $\mathbf{B}_m \in \Re^{n_a \times n_a}$ symbolises the motor inertia matrix and $\mathbf{D}_m \in \Re^{n_a \times n_a}$ expresses the motor damping matrix.

From (11), (12), (13), and (14) in static condition, i.e. $\dot{\boldsymbol{q}}_a = \ddot{\boldsymbol{q}}_a = \dot{\boldsymbol{\theta}} = \ddot{\boldsymbol{\theta}} = \mathbf{0}$, one can extract the desired motor positions vector as follows (see [43] for details)

$$\boldsymbol{\theta}_d = \boldsymbol{q}_d + \mathbf{K}_t^{-1}\boldsymbol{\tau_g}(\boldsymbol{q}). \tag{15}$$

2.4 Whole body Control Scheme

Higher-level tasks, such as operational-space position and orientation tasks, can be resolved via an inverse kinematics scheme. However, to ensure the compatibility of the joint-space solutions with the current/desired support state of the system, we include the set of contact constraints (6), and/or other crucial constraints with the highest priority in the inverse kinematics scheme. As a result, all higher-level tasks are projected to the null-space of the constraints Jacobian. It reads as

$$\dot{\boldsymbol{q}} = -\mathbf{J}_c^+\boldsymbol{e}_c \tag{16}$$

with $\boldsymbol{e}_c \triangleq \mathbf{0} \in \Re^k$ representing the constraints task error. The initial contact state is set from a default configuration; while it is updated online on the basis of variations in the robot contact state. Furthermore, additional contact points can be added or/and removed from the constraints task if unpredicted contact points occur.

The operational-space position and orientation tasks can be defined for state regulation of any point on the robot body, e.g. leg end-effectors. For a set of tasks determining the spatial position of $s \in \mathbb{N}$ points/frames, it is shown by

$$\dot{\boldsymbol{q}} = -\mathbf{J}_p^+\mu_p\boldsymbol{e}_p \tag{17}$$

where $\mathbf{J}_p \in \Re^{3s \times n}$ symbolises the task Jacobian, $\mu_p \in \Re^{3s \times 3s} = \text{diag}([\mu_1, ..., \mu_{3s}])$ stands for a tuning matrix, and $\boldsymbol{e}_p = [\boldsymbol{e}_1^T, ..., \boldsymbol{e}_s^T]^T$ expresses the task error. For position tracking, the task error reads as

$$\forall i \in \{1, \ldots, s\} : \boldsymbol{e_i} = \boldsymbol{x}_{i,des} - \boldsymbol{x}_i. \tag{18}$$

On the other hand, the orientation task is defined with quaternions, and thus a task error is expressed by [30]

$$\forall i \in \{1, \ldots, s\} : \boldsymbol{e_i} = w_i\boldsymbol{v}_{i,des} - w_{i,des}\boldsymbol{v}_i - \boldsymbol{v}_{i,des} \times \boldsymbol{v}_i \tag{19}$$

where a general quaternion is defined as $\boldsymbol{\rho} = [w, \boldsymbol{v}^T]^T$ with $w \in \Re^1$ symbolising the quaternion scalar part and $\boldsymbol{v} \in \Re^3$ referring to the quaternion vector part.

Multiple position and orientation tasks can be specified with different priorities; each can control aset of points/frames defined by reference frames attached to the robot body. Moreover, the definition of a point/frame in its reference frame can be updated online, without a need to redefine the whole task. This is useful for contact points as they do not have fixed frames on the robot.

2.5 Balancing

The balancing problem is addressed in this section by employing the generality of the developed control scheme. According to the definition in [44], a mechanical system is statically balanced when its centre of mass projection on the ground is within the convex support polygon confined by the supporting feet. Therefore, a whole-body CoM regulation task has been implemented at the velocity level. It is integrated into the aforesaid control scheme by defining the corresponding task as follows

$$\dot{\boldsymbol{q}} = -\mathbf{J}_{CoM}^{+} \mu_{CoM} \left(\boldsymbol{X}_{CoM,des} - \boldsymbol{X}_{CoM} \right), \tag{20}$$

where $\mu_{CoM} \in \Re^{2\times 2}$ represents a tuning matrix, $\mathbf{J}_{CoM} \in^{2\times n}$ is the whole-body CoM Jacobian determined using the sum of CoM Jacobians ($^{i}\mathbf{J}_{CoM}$) of robot parts weighted by their masses (m_j)

$$\mathbf{J}_{CoM} = \sum_{j=0}^{h} \frac{^{j}\mathbf{J}_{CoM}}{m_j} \tag{21}$$

with $h \in \mathbb{N}$ denoting number of robot parts.

2.6 Simulation Results

2.6.1 Pelvis Regulation

The control scheme has been evaluated in this section via simulation experiments on the CENTAURO lower-body, when regulating the robot pelvis height. In this test, a set of step trajectories were sent to the controller in operational space, assigning the desired pelvis height, as demonstrated in Fig. 4.

Results with and without the centralised controller are presented in Figs. 5 and 6 with the former showing the execution of the given task in the operational space, and the latter presenting the front left knee pitch tracking error on the motor and link sides. The minimum pelvis height for the system without the centralised controller (Fig. 5a) is 45 cm, while with the addition of the centralised controller it can go down to 40 cm (Fig. 5b). It is due to a fact that the system

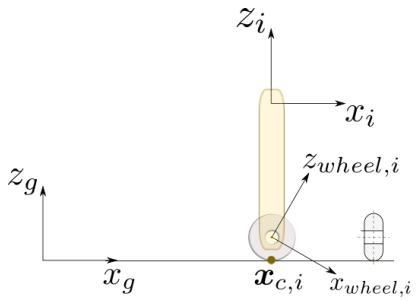

Figure 3: Scheme of the leg end-effector in the singular configuration.

without the centralised controller cannot correctly hold the position, and starts destabilising at this configuration. Fig. 6a shows that although the decentralised controller correctly drives the tracking error on the motor-side to zero, displacements due to the gravity effect causes steady-state position errors on the link-side.

2.6.2 Balancing

In this section, the validity of the CoM regulation approach is presented in a simulation when

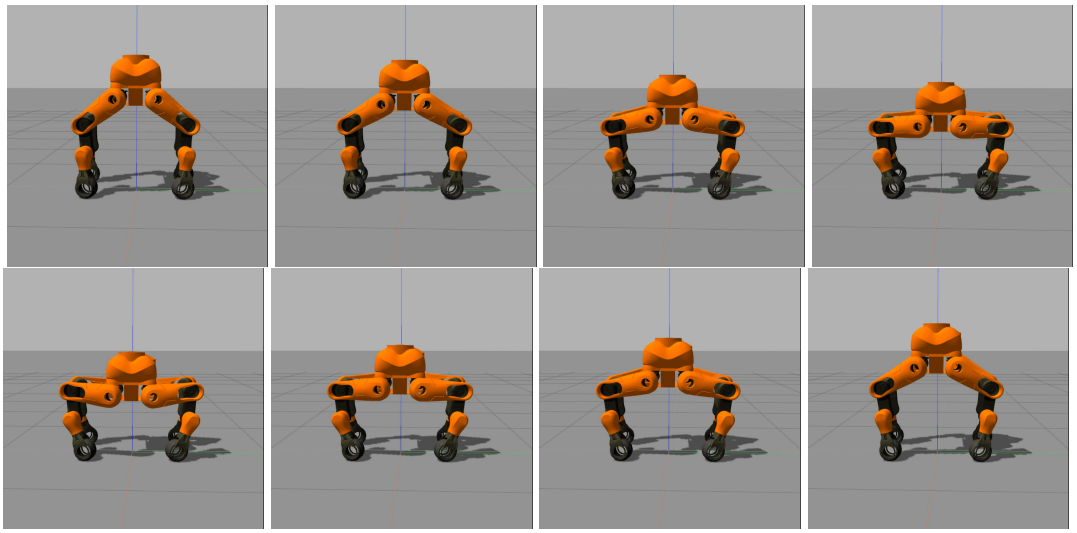

Figure 4: Robot executing the height regulation task.

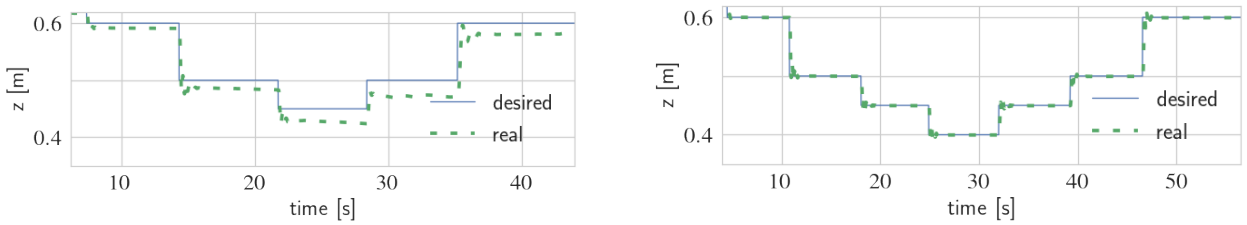

(a) without centralised controller

(b) with centralised controller

Figure 5: Operational space tracking error for the height regulation task

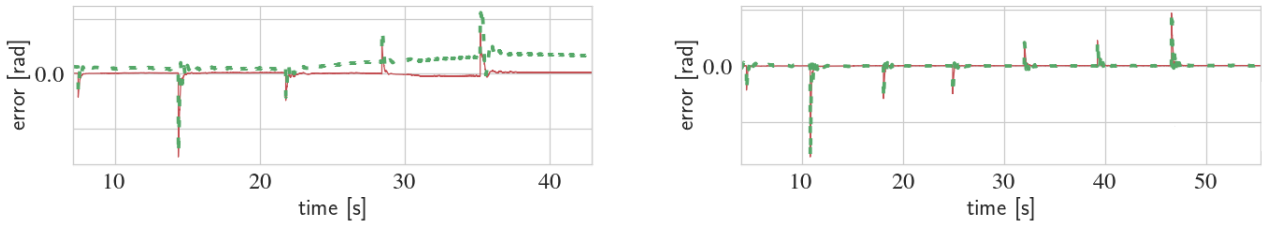

(a) without centralised controller

(b) with centralised controller

Figure 6: Joint space tracking error of the left front knee pitch joint for the height regulation task: motor-side and link-side position error are shown, respectively, in red line, and greed dash lines.

commanding the robot to move its CoM along a circular trajectory of 12 cm radius, and to maintain its height, while legs keep the ground contacts. Figure 7 presents a few poses of the robot when executing the above-said trajectories, and Fig. 8 shows the CoM position tracking results.

3 Wheeled motion

Motion control design for a platform with steerable wheels has to address a singularity problem occurring when the wheel camber and caster angles are zero. In this case, the wheel steering motion cannot be resolved by only using the aforementioned contact point assumption, and a

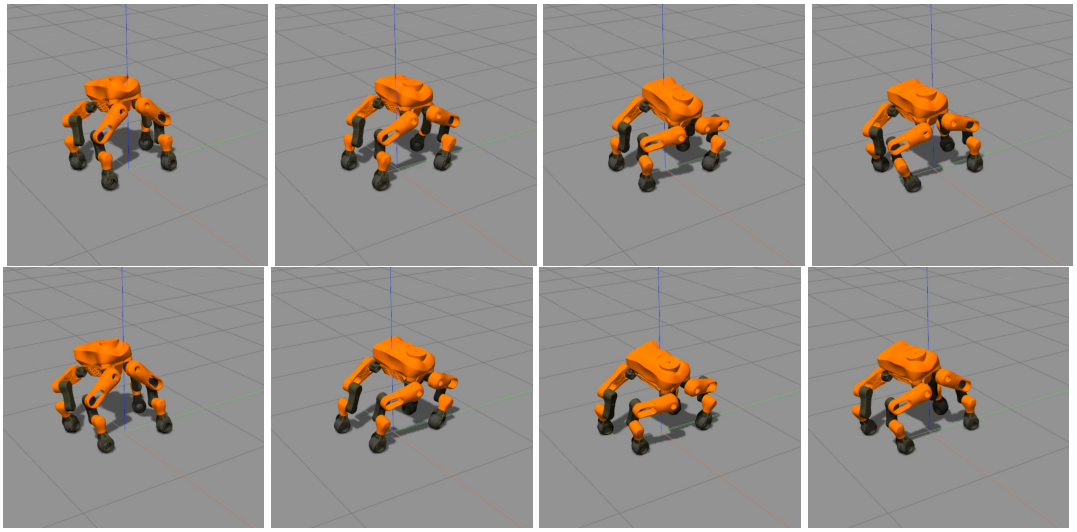

Figure 7: Robot performing the CoM tracking for a 12 cm-radius-circular-trajectory.

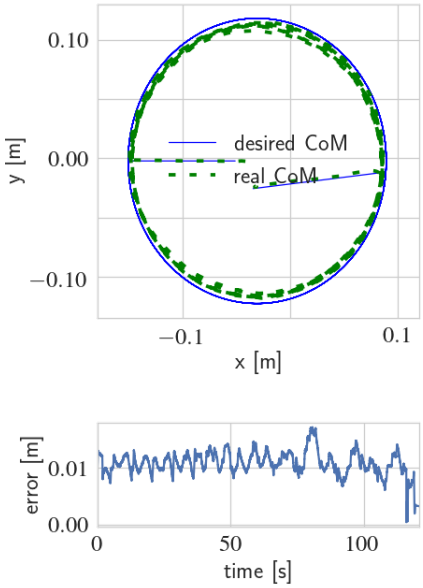

Figure 8: Centre of mass tracking error for the CoM regulation task.

non-holonomic constraint has to be satisfied to move a system with constant support polygon. To coordinate a steering motion in a way that it complies with the non-holonomic constraint, [33] and [6] proposed switching between walking and driving modes. [14] and [13] propounded to separate the ankle yaw and body posture kinematics, and solve the former for a desired steering angle. Furthermore, [12, 28, 29, 42] utilised a second order kinematic model described by both velocities and accelerations. The work in [10], however, employed the instantaneous centre of rotation (ICR) concept. The steering motion control of legged-wheeled systems highly inherit from their more extensively studied standard predecessors. To control all-steerable mobile robots, the literature has widely examined modelling with ICR [4, 5, 8, 35, 37]. It is often in combination with artificial potential fields method to avoid singularities [7, 34]. .

3.1 Driving mode through inverse kinematics control

The first-order kinematic model of a leg-wheeled platform is derived to solve the constraints equation (6) for the pelvis frame coordinates [13]. In this work the floating base model with the prioritised inverse kinematics is used, so that the positioning is carried out when the constraints task (16) are carried out at the highest priority level. Then, the system is controlled through the position and orientation tasks (17) defined at the pelvis reference frame. Choosing the floating base as the reference frame, the position $\mathbf{J}_{p,pelvis}$ and orientation $\mathbf{J}_{q,pelvis}$ tasks Jacobians are

$$\mathbf{J}_{p,pelvis} = \begin{bmatrix} \mathbf{I}^{3\times 3} & \mathbf{0}^{3\times(3+n_a)} \end{bmatrix}, \tag{22}$$

$$\mathbf{J}_{q,pelvis} = \begin{bmatrix} \mathbf{0}^{3\times 3} & \mathbf{I}^{3\times 3} & \mathbf{0}^{3\times n_a} \end{bmatrix}. \tag{23}$$

To additionally control the support polygon, a task on the wheels centres along the x and y coordinates $\boldsymbol{X}_{wheels} \in \Re^{2f}$ is added

$$\dot{\boldsymbol{q}} = \mathbf{J}^{+}_{wheels}\dot{\boldsymbol{X}}_{wheels} \tag{24}$$

with $\mathbf{J}_{wheels} \in \Re^{2f\times n}$ standing for the corresponding Jacobian matrix in a form

$$\mathbf{J}_{wheels} = \begin{bmatrix} \mathbf{J}_{wheels1} & \mathbf{J}_{wheels2} \end{bmatrix} \triangleq \begin{bmatrix} \mathbf{J}_{wheels1} & \mathbf{0} \end{bmatrix}. \tag{25}$$

where $\mathbf{J}_{wheels2} \in \Re^{2f}$ refers to the part of Jacobian related to the steering and driving DoFs, and $\mathbf{J}_{wheels1} \in \Re^{n-2f}$ expresses the remaining part of the Jacobian.

The solution can then be found through the inverse kinematics scheme; except for when the axis of an ankle yaw axis is perpendicular to the ground (Figure 3) and thus the constraints Jacobian (8) takes the following form

$$\mathbf{J}_c = \begin{bmatrix} \mathbf{J}_{c1} & \mathbf{0} & \mathbf{J}_{c3} \end{bmatrix}. \tag{26}$$

From (22), (23), (25) and (26), one can see, in this joints arrangement, the ankle yaw motion has no direct influence on any of the active tasks. In consequence, the inverse kinematics solution for the steering joints, at the singularity and in its proximity, yields zero velocity when there is enough degree of redundancy to exclude singular joints; otherwise, it results in unbounded velocity commands.

However, in contrary to standard all-steerable mobile robots, the kinematics of the CENTAURO legged-wheeled platform cannot be considered truly non-holonomic in such singular configuration. Articulated leg structure allows it to execute any pelvis/CoM motion

regardless of wheels' orientations. This motion may be provided without support polygon modification via legged motion, or with adjusting the support polygon through legged and/or driving motions [12]. However, in driving mode, workspace limitations heavily restrict the set of reachable pelvis/CoM states, and eventually the system kinematics become non-holonomic at the workspace edge.

One way to overcome this issue is to control the system in a way that it avoids stopping at singularity throughout a motion; although, this approach would greatly restrict robot workspace. Another approach is to consider the system to be always in singularity and solve the problem through the second-order kinematic model extending methods developed for all-steerable mobile robots (e.g. [41], [38]) as done in [42]. However, this approach also limits the workspace, and can lead to an invalid model for a leg far from singularity. In addition, it leads to a mixed velocity/acceleration state disturbing optimisation process for redundant systems.

3.2 Steering strategy

In this section, a strategy to coordinate the steering motion has been developed based on the ICR concept, that expresses a geometric constraint on the system to move as a rigid body.

Considering the system moving on a flat ground, a standard way to define ICR is to express it in a robot reference frame ($\boldsymbol{X}_{ICR}^{(r)}$) with respect to a desired pelvis velocity [8]

$$\boldsymbol{X}_{ICR}^{(r)} = \begin{bmatrix} \dfrac{\dot{x}_p^{(g)} \sin\left(\phi_r^{(g)}\right) - \dot{y}_p^{(g)} \cos\left(\phi_r^{(g)}\right)}{\dot{\phi}_r^{(g)}} \\ \dfrac{\dot{x}_p^{(g)} \cos\left(\phi_r^{(g)}\right) + \dot{y}_p^{(g)} \sin\left(\phi_r^{(g)}\right)}{\dot{\phi}_r^{(g)}} \end{bmatrix} \tag{27}$$

where $\phi_p^{(g)}$ denotes current pelvis heading.

However, if a desired angular velocity is zero, a modelling singularity emerges as the ICR is placed at infinity. To overcome this issue, a few authors (e.g. [12, 38]) computed the steering angle directly by solving the constraints for a mobile platform as

$$\beta_{i,des} = \arctan\left(\frac{-\sin(\phi_r)\dot{x}_{r,des} + \cos(\phi_r)\dot{y}_{r,des} + x_{ci}\dot{\phi}_{r,des}}{\cos(\phi_r)\dot{x}_{r,des} + \sin(\phi_r)\dot{y}_{r,des} + y_{ci}\dot{\phi}_{r,des}}\right) \tag{28}$$

with X_{ci} denoting coordinates of a i^{th} contact point.

Note that (27) and (28) rely only on the pelvis planar motion even though the legged-wheeled system can move in 3D. However, for non-planar motions, commanding the system to move as a rigid body contradicts the ground contacts constraints, and therefore we exploit the articulation of legs to compensate for the non-planar motions.

In case of legged-wheeled systems, the above equation does not fully represent the system constraints, and additional components representing variations in the support polygon have to be taken into account, thereby leading to a general solution

$$\beta_{i,des} = \arctan\left(\frac{f\left(\boldsymbol{q}, \dot{\boldsymbol{X}}_{r,des}, \dot{\phi}_{r,des}, \dot{\boldsymbol{X}}_{ci,des}\right)}{g\left(\boldsymbol{q}, \dot{\boldsymbol{X}}_{r,des}, \dot{\phi}_{r,des}, \dot{\boldsymbol{X}}_{ci,des}\right)}\right), \tag{29}$$

as reported in [42]. When applying a steering reference obtained from the constraints directly to the impedance controller at ankle yaw causes the support polygon to diverge when using the first order inverse kinematics.

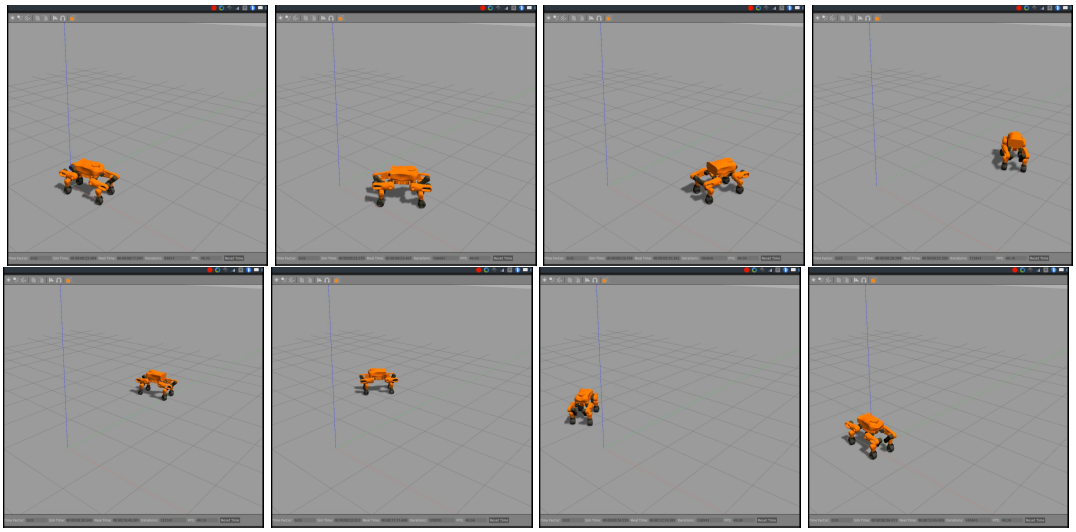

Figure 9: Robot following a 2 m-radius-circular-trajectory with wheeled motion.

Nevertheless, (28) is a valid equation for legged-wheeled systems and generates the desired wheel orientation for a robot moving with a fixed support polygon. Due to the redundant nature of the CENTAURO robot kinematics, this equation does not have to be fulfilled at each time instance to ensure tracking of the body/pelvis reference. Moreover, as it depends only on the desired pelvis planar velocities and the current wheel position, any inaccuracy in tracking of the computed reference will accumulate through the motion, thereby causing the support polygon to diverge. To compensate for the accumulated errors, and to ensure the global stability of the system, a regulation action on the wheel positions is added to the ICR steering strategy. Furthermore, the wheels camber angles are kept at zero during the wheeled motion so that their rotation axes are parallel to the ground, allowing for a continuous long-distant wheeled motion. Finally, the same strategy can be used to modify the support polygon with respect to the pelvis and in the world frame, regardless of the desired pelvis motion.

3.3 Results

The wheeled motion was tested on the CENTAURO simulator by commanding the robot to follow a 2 m-radius-circular-trajectory. In this test, the pelvis desired velocity was gradually increased, with a 0.1 rad/s step, from an initial value of 0.05 rad/s to a final value of 0.55 rad/s. Figure 9 depicts the robot performing the aforesaid task in simulation, Fig. 10 illustrated the desired and executed pelvis positions as well as the pelvis tracking error, and Fig. 11 presents the wheels tracking errors. The bottom plot of the Fig. 10 and Fig. 11 demonstrate noticeable step changes in tracking error, and are correlated with the desired velocity modifications.

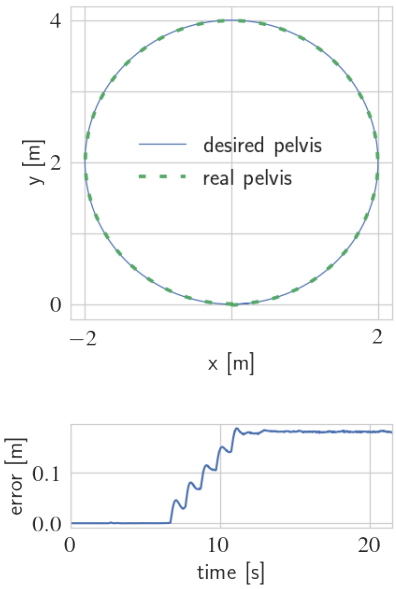

Figure 10: Pelvis desired and executed positions (upper plot) and pelvis tracking error (bottom plot) for the system following a 2 m-radius-circular- trajectory with the wheeled motion.

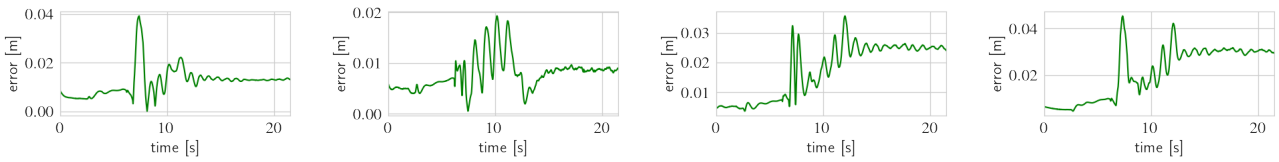

(a) front left wheel (b) front right wheel (c) rear left wheel (d) rear right wheel

Figure 11: Wheel tracking error for system following the 2 m radius circle with the wheeled motion.

4 Conclusions

In this report we introduced the concept details of the balancing control and wheeled locomotion approach for the CENTAURO robot. We presented the details of the whol-body controller serving for the robot balancing relying upon regulation of the COM position. The incorporation series elasticity into actuators are taking into account for both gravity compensation and state regulation. The Wheeled locomotion control scheme is carried out via steering strategies. It is based on the kinematics control of the robot defining the reference trajectories for the COM controller performing the robot balancing. This report presented an overview of the controllers, and finally, illustrate the performance of the proposed scheme in executing balancing, and tracking various locomotion trajectories through wheel motions.

References

[1] F. Aghili. Inverse and direct dynamics of constrained multibody systems based on orthogonal decomposition of generalized force. In *2003 IEEE International Conference on Robotics and Automation (Cat. No.03CH37422)*, volume 3, pages 4035–4041 vol.3, September 2003.

[2] F. Aghili. A unified approach for inverse and direct dynamics of constrained multibody systems based on linear projection operator: applications to control and simulation. *IEEE Transactions on Robotics*, 21(5):834–849, October 2005.

[3] V. Barasuol, J. Buchli, C. Semini, M. Frigerio, E. R. De Pieri, and D. G. Caldwell. A reactive controller framework for quadrupedal locomotion on challenging terrain. In *2013 IEEE International Conference on Robotics and Automation (ICRA)*, pages 2554–2561, May 2013. 00065.

[4] S. Chamberland, Beaudry, L. Clavien, F. Kabanza, F. Michaud, and M. Lauriay. Motion planning for an omnidirectional robot with steering constraints. In *2010 IEEE/RSJ International Conference on Intelligent Robots and Systems*, pages 4305–4310, October 2010.

[5] L. Clavien, M. Lauria, and F. Michaud. Instantaneous centre of rotation estimation of an omnidirectional mobile robot. In *2010 IEEE International Conference on Robotics and Automation*, pages 5435–5440, May 2010.

[6] Curtis L. Collins. Stiffness Modeling and Force Distribution for the All-Terrain Hex-Limbed Extra-Terrestrial Explorer (ATHLETE). pages 781–789, January 2007.

[7] C. P. Connette, C. Parlitz, M. Hagele, and A. Verl. Singularity avoidance for over-actuated, pseudo-omnidirectional, wheeled mobile robots. In *2009 IEEE International Conference on Robotics and Automation*, pages 4124–4130, May 2009.

[8] C. P. Connette, A. Pott, M. Hagele, and A. Verl. Control of an pseudo-omnidirectional, non-holonomic, mobile robot based on an ICM representation in spherical coordinates. In *2008 47th IEEE Conference on Decision and Control*, pages 4976–4983, December 2008.

[9] A. Dietrich, T. Wimbck, and A. Albu-Schffer. Dynamic whole-body mobile manipulation with a torque controlled humanoid robot via impedance control laws. In *2011 IEEE/RSJ International Conference on Intelligent Robots and Systems*, pages 3199–3206, September 2011.

[10] A. Dietrich, T. Wimbck, A. Albu-Schffer, and G. Hirzinger. Singularity avoidance for nonholonomic, omnidirectional wheeled mobile platforms with variable footprint. In *2011 IEEE International Conference on Robotics and Automation*, pages 6136–6142, May 2011.

[11] Roy Featherstone. Quantitative Measures of a Robots Ability to Balance. In *Proceedings of Robotics: Science and Systems*, 2015.

[12] P. R. Giordano, M. Fuchs, A. Albu-Schaffer, and G. Hirzinger. On the kinematic modeling and control of a mobile platform equipped with steering wheels and movable legs. In *2009 IEEE International Conference on Robotics and Automation*, pages 4080–4087, May 2009.

[13] Christophe Grand, Faiz Benamar, and Frdric Plumet. Motion kinematics analysis of wheeledlegged rover over 3d surface with posture adaptation. *Mechanism and Machine Theory*, 45(3):477–495, March 2010.

[14] Christophe Grand, Faz Benamar, Frdric Plumet, and Philippe Bidaud. Stability and traction optimization of a reconfigurable wheel-legged robot. *The International Journal of Robotics Research*, 23(10-11):1041–1058, 2004. 00132.

[15] A. Herzog, L. Righetti, F. Grimminger, P. Pastor, and S. Schaal. Balancing experiments on a torque-controlled humanoid with hierarchical inverse dynamics. In *2014 IEEE/RSJ International Conference on Intelligent Robots and Systems (IROS 2014)*, pages 981–988, September 2014. 00042.

[16] Marco Hutter, Hannes Sommer, Christian Gehring, Mark Hoepflinger, Michael Bloesch, and Roland Siegwart. Quadrupedal locomotion using hierarchical operational space control. *The International Journal of Robotics Research*, May 2014.

[17] S. h Hyon and G. Cheng. Passivity-Based Full-Body Force Control for Humanoids and Application to Dynamic Balancing and Locomotion. In *2006 IEEE/RSJ International Conference on Intelligent Robots and Systems*, pages 4915–4922, October 2006.

[18] S. H. Hyon, R. Osu, and Y. Otaka. Integration of multi-level postural balancing on humanoid robots. In *IEEE International Conference on Robotics and Automation, 2009. ICRA '09*, pages 1549–1556, May 2009. 00037.

[19] N. Kashiri, L. Baccilere, L. Muratore, and N. Tsagarakis. Deliverable D2.2 Prototype of Upper Body of CENTAURO Robot. Technical report, 2016.

[20] O. Khatib. A unified approach for motion and force control of robot manipulators: The operational space formulation. *IEEE Journal on Robotics and Automation*, 3(1):43–53, February 1987.

[21] J. Z. Kolter, M. P. Rodgers, and A. Y. Ng. A control architecture for quadruped locomotion over rough terrain. In *IEEE International Conference on Robotics and Automation, 2008. ICRA 2008*, pages 811–818, May 2008. 00116.

[22] M. de Lasa and M. Buehler. Dynamic compliant quadruped walking. In *IEEE International Conference on Robotics and Automation, 2001. Proceedings 2001 ICRA*, volume 3, pages 3153–3158 vol.3, 2001.

[23] Sung-Hee Lee and Ambarish Goswami. A momentum-based balance controller for humanoid robots on non-level and non-stationary ground. *Auton Robot*, 33(4):399–414, April 2012. 00075.

[24] C. Liu and C. G. Atkeson. Standing balance control using a trajectory library. In *IEEE/RSJ International Conference on Intelligent Robots and Systems, 2009. IROS 2009*, pages 3031–3036, October 2009. 00057.

[25] Guanfeng Liu and Zexiang Li. A unified geometric approach to modeling and control of constrained mechanical systems. *IEEE Transactions on Robotics and Automation*, 18(4):574–587, August 2002.

[26] Jian Meng, Yibin Li, and Bin Li. A Dynamic Balancing Approach for a Quadruped Robot Supported by Diagonal Legs. *International Journal of Advanced Robotic Systems*, page 1, 2015.

[27] M. Mistry, J. Buchli, and S. Schaal. Inverse dynamics control of floating base systems using orthogonal decomposition. In *2010 IEEE International Conference on Robotics and Automation*, pages 3406–3412, May 2010.

[28] K. Nagano and Y. Fujimoto. A control method of low speed wheeled locomotion for a wheel-legged mobile robot. In *2014 IEEE 13th International Workshop on Advanced Motion Control (AMC)*, pages 332–337, March 2014.

[29] K. Nagano and Y. Fujimoto. The stable wheeled locomotion in low speed region for a wheel-legged mobile robot. In *2015 IEEE International Conference on Mechatronics (ICM)*, pages 404–409, March 2015.

[30] Jun Nakanishi, Rick Cory, Michael Mistry, Jan Peters, and Stefan Schaal. Operational Space Control: A Theoretical and Empirical Comparison. *The International Journal of Robotics Research*, 27(6):737–757, June 2008.

[31] Marko B. Popovic, Ambarish Goswami, and Hugh Herr. Ground reference points in legged locomotion: Definitions, biological trajectories and control implications. *The International Journal of Robotics Research*, 24(12):1013–1032, 2005. 00241.

[32] H. Sadeghian, L. Villani, M. Keshmiri, and B. Siciliano. Task-Space Control of Robot Manipulators With Null-Space Compliance. *IEEE Transactions on Robotics*, 30(2):493–506, April 2014.

[33] Max Schwarz, Tobias Rodehutskors, Michael Schreiber, and Sven Behnke. Hybrid Driving-Stepping Locomotion with the Wheeled-legged Robot Momaro. 00001.

[34] U. Schwesinger, C. Pradalier, and R. Siegwart. A novel approach for steering wheel synchronization with velocity/acceleration limits and mechanical constraints. In *2012 IEEE/RSJ International Conference on Intelligent Robots and Systems*, pages 5360–5366, October 2012.

[35] M. F. Selekwa and J. R. Nistler. Path tracking control of four wheel independently steered ground robotic vehicles. In *2011 50th IEEE Conference on Decision and Control and European Control Conference*, pages 6355–6360, December 2011.

[36] A. Shkolnik and R. Tedrake. Inverse Kinematics for a Point-Foot Quadruped Robot with Dynamic Redundancy Resolution. In *Proceedings 2007 IEEE International Conference on Robotics and Automation*, pages 4331–4336, April 2007.

[37] M. Sorour, A. Cherubini, P. Fraisse, and R. Passama. Motion Discontinuity-Robust Controller for Steerable Mobile Robots. *IEEE Robotics and Automation Letters*, 2(2):452–459, April 2017.

[38] M. Sorour, A. Cherubini, R. Passama, and P. Fraisse. Kinematic modeling and singularity treatment of steerable wheeled mobile robots with joint acceleration limits. In *2016 IEEE International Conference on Robotics and Automation (ICRA)*, pages 2110–2115, May 2016.

[39] B. Stephens. Integral control of humanoid balance. In *IEEE/RSJ International Conference on Intelligent Robots and Systems, 2007. IROS 2007*, pages 4020–4027, October 2007.

[40] B. Stephens and C. Atkeson. Modeling and control of periodic humanoid balance using the Linear Biped Model. In *2009 9th IEEE-RAS International Conference on Humanoid Robots*, pages 379–384, December 2009.

[41] C. Stger, A. Mller, and H. Gattringer. Kinematic analysis and singularity robust path control of a non-holonomic mobile platform with several steerable driving wheels. In *2015 IEEE/RSJ International Conference on Intelligent Robots and Systems (IROS)*, pages 4140–4145, September 2015.

[42] A. Suzumura and Y. Fujimoto. Workspace control of a wheel-legged mobile robot for gyrating locomotion with movable leg. In *2013 IEEE International Conference on Mechatronics (ICM)*, pages 641–647, February 2013.

[43] P. Tomei. A simple PD controller for robots with elastic joints. *IEEE Transactions on Automatic Control*, 36(10):1208–1213, October 1991. 00360.

[44] Pierre-Brice Wieber, Russ Tedrake, and Scott Kuindersma. Modeling and Control of Legged Robots. In *Springer Handbook of Robotics*, pages 1203–1234. Springer, Cham, 2016. DOI: 10.1007/978-3-319-32552-1_48.